Influence of Bulk Elasticity and Interfacial Tension on the Deformation of Gelled Water-in-Oil Emulsion Droplets: An AFM Study

D. Filip,* V. I. Uricanu, M. H. G. Duits, W. G. M. Agterof, and J. Mellema

Physics of Complex Fluids group, University of Twente, Faculty of Science and Technology, associated with the J. M. Burgerscentrum for Fluid Mechanics, and Institute of Mechanics, Processes and Control - Twente (IMPACT), Postbus 217, 7500 AE Enschede, The Netherlands

Received July 9, 2004. In Final Form: October 15, 2004

We used atomic force microscopy (AFM) to study the deformation and wetting behavior of large (50−250 μm) emulsion droplets upon mechanical loading with a colloidal glass probe. Our droplets were obtained from water-in-oil emulsions. By adding gelatin to the water prior to emulsification, also droplets with a bulk elasticity were prepared. Systematic variations of surfactant and gelatin concentrations were made, to investigate their effect on the deformation and wetting behavior of the droplets and to identify the contributions of interfacial tension, bulk elasticity, and expelled water. The AFM experiments were performed in force−distance mode and showed on approach a repulsive regime which in many cases was terminated by a jump-in of the probe. In the case of pure water (i.e. gelatin-free) droplets, the repulsive part of the curve showed a good linearity, thus allowing the extraction of an effective droplet spring constant. This quantity was found to decrease on raising the surfactant concentration from below the critical micelle concentration (cmc) to well above the cmc, and its numerical values were found to correspond remarkably well to literature values for the interfacial tension. Our findings indicate that, on gelatin increase inside the droplets, the bulk elasticity gradually becomes dominant and the droplets' stiffness does not depend anymore on surfactant concentration. Also the stability of the droplet interface against wetting, as measured by the force at which the jump-in instability occurs, was enhanced by gelatin. For gelatin concentrations of ≥15 wt %, the droplets were found to behave like purely elastic bodies. Both gelatin and surfactant contribute positively to the stability against interface breakup.

1. Introduction

Emulsions form the basis of a wide variety of natural and manufactured materials, including food products, pharmaceuticals, biological fluids, agrochemicals, petrochemicals, cosmetics, and so forth.[1] Some products such as margarine or mayonnaise may contain a high volume fraction (up to 90%) of dispersed droplets of one immiscible phase into another one. Comparing these volume fractions to typical maximum packing fractions for *rigid spheres*, it is implied that in concentrated *emulsions*, large droplet deformations must occur. The mechanical properties in such systems are set by an interplay between colloidal forces and forces due to the droplet deformability. When droplets deform as a consequence of colloidal forces, then these forces change as well, due to the modified surface distance and area involved. The consequences of this mutual dependence can be different. As long as colloidal *repulsions* dominate, the deformability will enhance the prevention of interdroplet contacts improving stability against aggregation and coalescence. However when the colloidal *attractions* dominate, the deformability will allow a larger contact area, thus increasing the adhesion strength. In practice this means that the stability of an emulsion can be drastically changed by manipulating the elasticity of the *droplet inner phase*. However, only a few studies have so far been aimed to a closer look into the interplay between colloidal and elastic forces.

One powerful technique for studying colloidal interactions and the deformation in soft materials is atomic force microscopy (AFM). After Ducker et al.[2] reported the use of a colloidal particle attached to the cantilever to probe surface forces, Butt[3] was the first to study the deformation of bubbles and droplets under compression by a colloidal probe. Since then, several studies were reported for bubbles[4−11] and oil droplets in aqueous surroundings.[12−18]

Also theoretical studies on the deformation of pinned (to a substrate) droplets or bubbles, under mechanical loading with an AFM spherical indenter, were reported. Attard and Miklavcic[19,20] derived that the "spring constant", as defined from the slope of an AFM force−distance curve, is almost equal to the interfacial tension. The forces

* To whom correspondence should be addressed. E-mail: d.filip-boar@tnw.utwente.nl.

(1) *Encyclopedia of emulsion technology*, *Vol. 2*; Becher, P., Ed.; Marcel Dekker: New York, 1985.
(2) Ducker, W. A.; Senden, T. J.; Pashley, R. M. *Nature* **1991**, *353*, 239.
(3) Butt, H.-J. *J. Colloid Interface Sci.* **1994**, *166*, 109.
(4) Ducker, W. A.; Xu, Z.; Israelachvili, J. N. *Langmuir* **1994**, *10*, 3279.
(5) Fielden, M. L.; Hayes, R. A.; Ralston, J. *Langmuir* **1996**, *12*, 3721.
(6) Preuss, M.; Butt, H.-J. *Langmuir* **1998**, *14*, 3164.
(7) Carambassis, A.; Jonker, L. C.; Attard, P.; Rutland, M. W. *Phys. Rev. Lett.* **1998**, *80*, 5357.
(8) Ecke, S.; Preuss, M.; Butt, H.-J. *J. Adhes. Sci. Technol.* **1999**, *13*, 1181.
(9) Ralston, J.; Fornasiero, D.; Hayes, R. *Int. J. Miner. Process.* **1999**, *56*, 133.
(10) Yakubov, G. E.; Vinogradova, O. I.; Butt, H.-J. *Colloid J.* **2001**, *63*, 518.
(11) Nguyen, A. V.; Nalaskowski, J.; Miller, J. D. *Miner. Eng.* **2003**, *16*, 1173.
(12) Mulvaney, P.; Perera, J. M.; Biggs, S.; Grieser, F.; Stevens, G. W. *J. Colloid Interface Sci.* **1996**, *183*, 614.
(13) Basu, S.; Sharma, M. M. *J. Colloid Interface Sci.* **1996**, *181*, 443.
(14) Snyder, B. A.; Aston, D. E.; Berg, J. C. *Langmuir* **1997**, *13*, 590.
(15) Hartley, P. G.; Grieser, F.; Mulvaney, P.; Stevens, G. W. *Langmuir* **1999**, *15*, 7282.
(16) Aston, D. E.; Berg, J. C. *J. Colloid Interface Sci.* **2001**, *235*, 162.
(17) Aston, D. E.; Berg, J. C. *Ind. Eng. Chem. Res.* **2002**, *41*, 389.
(18) Nespolo, S. A.; Chan, D. Y. C.; Grieser, F.; Hartley, P. G.; Stevens, G. W. *Langmuir* **2003**, *19*, 2124.
(19) Attard, P.; Miklavcic, S. *Langmuir* **2001**, *17*, 8217.
(20) Attard, P.; Miklavcic, S. *J. Colloid Interface Sci.* **2002**, *247*, 255.

10.1021/la048276y CCC: $30.25
Published on Web 12/08/2004

between a rigid probe particle and a liquid interface were extensively analyzed by Chan et al.[21] and Dagastine.[22] The equilibrium shape of bubbles/droplets was determined by Bhatt et al.[23] using the augmented Young−Laplace equation. Bardos[24] gave an extensive analysis of how the contact angle between a pinned drop and the substrate depends on the *probe−drop* force in AFM measurements. Nespolo et al.[18] took into account the detailed expression of the disjoining pressure and calculated the complete force−distance curves using as input Derjaguin−Landau−Verwey−Overbeek (DLVO) type potentials.

To our knowledge, no experimental studies have yet been reported on *aqueous droplets in nonpolar media*, despite many industrial applications of such systems. In this paper, we report on AFM experiments on aqueous droplets in dodecane, with Span 80 being present as the surfactant. In the first part of the paper, we describe the behavior of typically viscous water droplets as a model system. The second part of the paper deal with aqueous but gelled elastic droplets. In this system, two types of stability can be defined. The first one is related to the *bond strength* between droplets which maintain their integrity. It is set by the colloidal attractions (e.g., van der Waals or polymer induced) and modulated by the droplet deformability. The second one is the stability of the droplet interface against *coalescence*. Commonly, this type of stability is achieved via a protective layer, created by emulsifiers, proteins, copolymers, and so forth, through adsorption at the water−oil interface. Considering the long-term stability or the stability under compression, such an interfacial barrier is not always strong enough to prevent coalescence of the droplets. Another method that could improve the stability is the addition of a gelling agent to the droplet phase. Gelatin stimulates the formation of an elastic network inside the droplets, which could lead to an increased resistance against interface breakup and coalescence.

Making use of the AFM capabilities, we analyze in the present paper the influence of both the bulk elasticity and interfacial strength against breakup of water-in-oil (W/O), elastic, gelled emulsion droplets. Up till now, only the paper of Gillies and Prestidge[25] focused on both these parameters, their samples being viscoelastic poly(dimethylsiloxane) (PDMS) droplets/particles in sodium dodecyl sulfate (SDS) aqueous solutions. A key ingredient in our study is the comparison between pure water droplets and gelled droplets having various degrees of gelation strength. By varying the surfactant content around the critical micelle concentration (cmc), we also varied the interfacial tension. A colloidal glass probe was used to compress into individual emulsion droplets. The diameter ratio between the droplet and the probe was chosen to be at least 10, so that the droplet interface can be regarded as a flat surface and the capillary pressure of the droplet does not play a significant role.

2. Theoretical Background

To describe the geometric configurations adopted locally by the interface (of two otherwise immiscible liquids) as an AFM probe advances toward it, both the colloidal interaction between probe and droplet (i.e., the disjoining pressure, Π) and the surface tension γ of the water-in-oil (W/O) interface are needed. Different mechanical regimes have been mentioned in the literature[19] and are briefly reviewed here. When the probe is so far away from the interface that no interaction between the two exists, the interface is undeformed. Approaching closer to the droplet, mutual probe−droplet interactions come into play and produce a local change in the droplet's curvature. If the equilibrium shape of the interface is concave, the curvature (J) is positive, while for convex curvatures J assumes negative values. The latter is anticipated for the regime addressed in the present study. The equilibrium shape of the interface is determined by the relative magnitudes of the disjoining pressure (Π, between the probe and the droplet) and the Laplace pressure (P = the difference in pressure between inside and outside the droplet). For our system of aqueous droplets in oil, the Laplace pressure can be written as $P = 2\gamma J$.

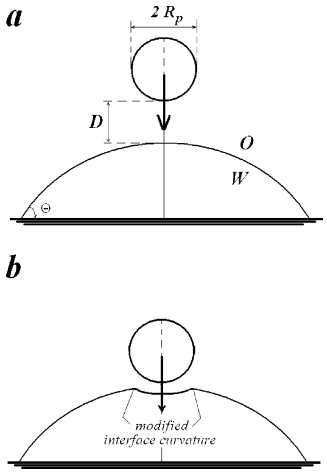

Figure 1. Snapshots of the geometry encountered during probe−drop AFM experiments, with the indenting (upper) glass bead far above the O/W interface (a) and in the wrapping regime (b). (The deformation is not shown to scale.)

As long as the pressure exerted by the probe is smaller than the sum (Π + P), a thin liquid layer is maintained between the glass indenter and the (deforming) droplet (see Figure 1a,b). For small enough pressures (or forces $F \ll 2\pi\gamma R_p$, with R_p the radius of the indenting probe), "wrapping" will occur. This refers to a compression regime in which the interface profile near the probe changes its curvature, to accommodate the probe (without rupture of the interface). For this to happen, the maximum in the disjoining pressure has to satisfy the condition

$$\Pi_{max} > 2\gamma\left(\frac{1}{R_p} + \frac{1}{R_0}\right) \quad (1)$$

with R_0 the drop's initial local radius of curvature along the vertical axis. If eq 1 is violated, the interaction becomes unstable and probe wetting occurs.

In the following, we will consider the regime where eq 1 is satisfied. Describing the modified interface profile with a parabola, and assigning a "wrapping radius" R_w to characterize the local curvature, R_w will change from $-R_0$ at small loads to R_p at larger loads. Assuming that the range of the repulsion which facilitates the wrapping can be characterized by a decay length κ^{-1} much smaller than R_p (i.e., $\kappa R_p \gg 1$), Attard and Miklavcic[19] derived that, on increasing the loading force (F), a (constant) minimum distance D_{min} between the probe and the (deformed) droplet interface is reached.

(21) Chan, D. Y. C.; Dagastine, R. R.; White, L. R. *J. Colloid Interface Sci.* **2002**, *236*, 141.
(22) Dagastine, R. R.; White, L. R. *J. Colloid Interface Sci.* **2002**, *247*, 310.
(23) Bhatt, D.; Newman, J.; Radke, C. J. *Langmuir* **2001**, *17*, 116.
(24) Bardos, D. C. *Surf. Sci.* **2002**, *517*, 157.
(25) Gillies, G.; Prestidge, C. A. *Adv. Colloid Interface Sci.* **2004**, *108−109*, 197.

Using an approximation of condition 1, these authors associated the minimum probe−droplet distance to a maximum disjoining pressure:

$$\Pi_{max}(D_{min}) \cong 2\gamma/R_p \quad (2)$$

and derived that any further compression will result in a linear relation between the loading force (F) and the indentation (δ) into the drop:

$$F = K_d\delta \quad (3)$$

where δ is measured along the droplet's central (vertical) axis and K_d is the effective spring constant of the droplet, given by

$$K_d^{-1} = \frac{-1}{4\pi\gamma}\left\{\ln\left[\frac{R_p}{2\kappa R_0^2}\frac{(1+\cos\theta)^2}{\sin^2\theta}\right] + \frac{4-5\cos\theta+2\cos^2\theta-\cos^3\theta}{2-\cos\theta-\cos^3\theta}\right\} \quad (4)$$

with θ the contact angle of the (pinned) droplet at the substrate.

The literature term *constant compliance regime* refers to the interface (and droplet) compression under condition 3.

For various oil/water systems, it was found that $K_d \cong \alpha\gamma$, with $\alpha \approx 1$ (maximum deviation, 20%). The dependence of K_d on R_p, R_0, κ, and θ turned out to be weak around the working points of the studies cited in ref 19. For systems with a repulsion other than electrostatic (e.g., contact in air), the boundary radius of the wrapping regime is different but the (almost) quantitative correspondence between the spring constant and the interfacial tension should be retained according to ref 19.

Application to an Aqueous Drop in Oil. Looking at eq 4, the question is, which repulsion type and with which corresponding decay length κ^{-1} is responsible for entering the wrapping regime. This κ^{-1} has to be used for predicting K_d from eq 4. We have attempted to estimate it for our system of a glass probe interacting with an aqueous drop in dodecane.

One possibility is that electrostatic interactions (i.e., likewise charged surfaces) provide a sufficiently strong repulsion. Calculating the Debye length however requires knowledge of the electrolyte concentration(s) in the dodecane. In view of the low dielectric constant of dodecane (i.e., 2.0), this can only involve small numbers of ions, which are difficult to measure. Instead of making a theoretical calculation, we have attempted to estimate a typical decay length κ^{-1} from our AFM force−distance curves. For pure water droplets, the ascendant part of the *cantilever deflection (D) versus piezo displacement (Z)* curve (from now on termed the $D-Z$ curve) showed deviations from "constant compliance" for piezo displacements between 30 and 200 nm, corresponding to ≈170 nm tip displacement, but this 170 nm could also include some droplet deformation. For the hard (glass) substrate, the $D-Z$ curve showed a typical nonlinear part of 30−50 nm. These numbers suggest a typical κ^{-1} ranging between 10 and 100 nm. Combining this with typical values of $R_p = 2.5 \times 10^{-6}$ m, $R_0 \approx 25-125 \times 10^{-6}$ m, and $\theta \approx 120-150°$, we obtain

$$K_d^{-1} \approx (0.55-1.09)\gamma^{-1} \quad \text{or} \quad K_d \approx (0.92-1.82)\gamma$$

In any case there will be a steric repulsion due to the (Span 80) surfactant adsorbed at the interface. Assuming that this repulsion determines the wrapping regime, a decay length $\kappa^{-1}$of 1−3 nm should be used, corresponding to

$$K_d^{-1} \approx (0.82-1.27)\gamma^{-1} \quad \text{or} \quad K_d \approx (0.79-1.22)\gamma$$

Table 1. Composition and Index of the Studied Emulsion Samples

surfactant concn in dodecane (mM)	samples index, aqueous phase: pure water	gelatin gels (wt % of the polymer in water): 5% gel	10% gel	15% gel	20% gel	30% gel
0.023	A1	B1	C1	D1		
0.12	A2	B2	C2	D2	E2	F2
0.17	A3[a]					
0.23	A4[a]	B4	C4	D4	E4	F4
1.16	A5[a]	B5	C5	D5		
2.33	A6[a]					

[a] Formulations for which spontaneous emulsification was seen (see details in the text).

3. Experimental Section

3.1. Materials and Sample Preparation. Analytical grade (99+% purity) dodecane was obtained from Aldrich. The Span 80 surfactant (sorbitane monooleate), purchased from Fluka, had an HLB value of 4.3. Gelatin powder (from alkali-treated source, isoelectric point at pH = 5 and Bloom strength of 180 g) was kindly provided by Delft Gelatin BV, The Netherlands.

Water-in-oil emulsions were prepared at 60 °C by slowly pouring a "water phase" into an "oil phase" while mixing with a magnetic stirrer at a speed of 1000 rpm for 5 min. The water phase consisted of either pure Milli-Q water or of a gelatin solution herein. Gelatin solutions were prepared as follows: a known amount of gelatin powder was left to soak in water for 30 min and was then kept for 1 h in an oven at 60 °C to dissolve the gelatin granules, after which the hot liquid solution was homogenized by stirring. The oil phase consisted of dodecane and Span 80 surfactant. Several oil phases were prepared, at different surfactant concentrations. To avoid gelation upon mixing, the oil phase was preheated to the same temperature as the gelatin solution. "Fresh emulsions" thus prepared were directly transferred to the AFM cell, as described below. Table 1 summarizes the formulations of the studied emulsion samples (1 wt % Span 80 = 23.3 mM).

The range of surfactant concentrations used in preparing the samples was adjusted according to observations done in preliminary experiments. For smaller (than 0.023 mM) surfactant concentration, the water phase has a high affinity for the AFM indenter and the recordings are disturbed by snap-into-contact jumps so large that the reflected laser beam does not fall on the detector anymore. On the other extreme, for larger amounts of Span 80 in the oil phase, spontaneous emulsification (SE) is stimulated even for the gelatin-containing droplets.

A few more comments are worthwhile to add regarding this last issue. In another study performed by us,[26] it was seen that, above certain threshold values of the Span 80 concentration, immersion of water or water/gelatin droplets under dodecane with Span 80 stimulates the formation of small (around 600 nm diameter) satellite droplets at the surface of the aqueous reservoirs. For the surfactant concentrations used in the present study, SE was observed only for a few samples (see Table 1). The extent of the SE process is far less than what was reported for high surfactant concentrations. Here only a small number of SE tiny droplets are formed and most of them tend to roll-over the curved surface of the mother-reservoirs, leaving a "clean" (free from satellites) interface between the oil and the aqueous phase. Measuring on clean interfaces excludes any possible extra-influence (on the AFM data) coming from SE.

(26) Uricanu, V. I.; Filip, D.; Nelissen, R. M. F.; Duits, M. H. G.; Agterof, W. G. M. Gelatine Gels/Dodecane Interfaces. II. Surfactant-Mediated Water Transport. Manuscript in preparation.

Glass slides were used as substrates to attach the emulsion droplets. Before mounting in the AFM liquid cell, the substrates were cleaned with piranha solution for 15 min, extensively washed afterward with water and ethanol, and dried under nitrogen. For each given formulation, a few hundred microliters of the emulsion were inserted (with a syringe) in the corresponding oil phase (1 mL, thermostated at room temperature) already placed in the AFM cell. All samples were left to equilibrate overnight as to allow the emulsion droplets to settle on the glass. Meanwhile, also the gelation process inside the gelatin-containing droplets progressed. In all cases, experiments were performed after 24 h from preparation, meaning that there are no differences in the aging history among our samples.

3.2. Methods. Home-built AFM equipment, based on the stand-alone principle,[27] was used to measure forces between a spherical indenter and individual water-based emulsion droplets in dodecane/Span 80. During experiments, the sample is kept immobile while the *xyz* piezoscanner makes controlled cantilever movements. For compression experiments, we used cantilevers having a spring constant $K_c = 0.1$ N/m, with attached borosilicate glass spheres (5.1 μm diameter) The roughness of these beads has been checked by the manufacturer, by ourselves with scanning electron microscopy (SEM), and by other users with AFM and indicated the absence of sharp substructures. The values of the spring constants were checked (using the thermal excitation spectrum) and found to agree with the ones given by the supplier (Novascan Technologies, Ames, IA). Before each experiment, the cantilever was rinsed thoroughly with ethanol and left to dry at room temperature. To allow thermal and adsorption equilibration, the cantilever was then immersed and left for 30 min in the oil phase, far above the substrate/droplets.

The results reported in the present paper are based on data acquisition during approach−retraction cycles with a constant velocity (in the *z*-direction), 4.6 μm/s, of the cantilever base. To explore the significance of hydrodynamic forces and/or droplet viscoelasticity, a few experiments with higher (up to 12.4 μm/s) velocities were performed. For gelatin-containing droplets, curves measured at the different speeds superimposed nicely. For one selected pure water droplet, it was observed that increasing the speed from 4.6 to 9.2 μm/s or higher led to a smaller initial slope of the $D-Z$ curve. However, for 3 nN or higher (i.e., the most relevant part of the curves for the present study, see section 4.1), the slopes became identical. Each AFM scan provided 256 $D-Z$ curves at different spots on an area of 1 μm^2 of the droplet. Prior to and after each set of experiments on the droplets of a given sample, the deflection sensitivity of the cantilever was determined by recording a few $D-Z$ curves on the bare glass substrate, in the same AFM cell.

Our AFM setup includes a built-in, inverted optical microscope with 10× magnification. This allows us to select the droplet and precisely position the cantilever above the droplet center. Moreover, it reassures that the measurements are done on droplets nonaffected by spontaneous emulsification.

In our AFM experiments, for each given composition, droplets with different diameters were sampled. To facilitate centering and to minimize capillary pressure effects, only large droplets (with diameters between 50 and 250 μm) were chosen. All droplets were observed with the microscope to maintain a circular cross section. Most of them appeared to be well attached to the substrate, as evidenced by the absence of droplet movement under compression with the AFM.

The few droplets that were *not* attached to the glass bottom showed a clear lateral movement under compression. Presumably, adhesion of these droplets was still prevented by a thin film of oil (plus surfactant). Figure 2 shows the image of a droplet and the cantilever (dark triangle-shaped), recorded with the CCD camera attached to the optical microscope. Due to its size, smaller than the cantilever width (≈20 μm), the colloidal probe is not visible in Figure 2.

4. Results and Discussion

4.1. Deformation of Water Droplets. 4.1.1. General Behavior. Systems A1−A6 (water droplets in dodecane with Span 80) showed similarities in their mechanical behavior upon loading with a glass probe. Some representative $D-Z$ curves, at different Span 80 concentrations, are presented in Figure 3.

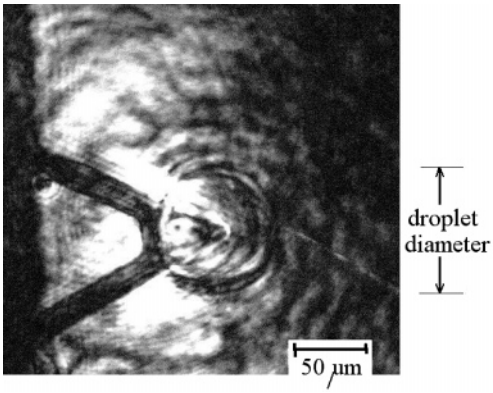

Figure 2. Optical (transmission) image of a triangular cantilever centered on the top of a water droplet.

At low Span 80 concentrations (≤0.12 mM), a strong attractive force caused the probe to jump into contact with the water droplet on almost all approaches (jump-in frequency, 90−100%). In a few cases (<10%), the interface showed a resistance before the jump-in (like in Figure 3a). The associated maximum force could reach values up to 3−5 nN.

On retraction, the force holding back the tip was so large that a piezo travel of 2 microns was insufficient to get out of contact. Snap-out had to be forced manually here. At a Span 80 concentration slightly above 0.12 mM, it was possible to obtain some curves without snap-in (jump-in frequency, about 30%). At much higher Span 80 concentrations (≥1.16 mM), the reverse was the case: only a few jump-ins (frequency, 10−20%) were observed, indicating a high resistance to breakup. Figure 3c2 gives an example where no jump-in is present even for compression with an equivalent force close to 9 nN. Curves such as this were observed many times and turned out to be highly reproducible, symmetric (i.e., without hysteresis between the approach and retraction cycles), and predominantly linear. For compression forces around 11 nN, the probe−droplet system appeared to be in a critical condition for jump-into-contact. Sometimes such a snap-into-contact happened during the *retraction* cycle; this is illustrated in Figure 3c1.

4.1.2. Approach Curves before Snap-In. In this regime, the physical interpretation of the $D-Z$ curves should be the least complicated, since no wetting has occurred yet. In this case, the probe interacts with the droplet through the dodecane/Span medium. We had a closer look on two main aspects. The first one concerns the stability of the intermediate oil layer, as measured by the maximum force F_{max} (the force associated with point C in Figure 5) experienced by the probe just before snap-into-contact with the water reservoir underneath. Inspecting many $D-Z$ curves measured on water droplets revealed that F_{max} depends on the Span 80 concentration but also shows an appreciable spread (see Figure 4).

On average, the maximum force preceding the *snap-in* grows with surfactant concentration. This is in accordance with expectation: raising the surfactant concentration leads to an increased adsorption at the interface, with the consequence that (a) the disjoining pressure becomes more repulsive at distances comparable to the size of the

(27) van der Werf, K. O.; Putman, C. A. J.; de Grooth, B. G.; Segerink, F. B.; Schipper, E. H.; van Hulst, N. F.; Greve, J. *Rev. Sci. Instrum.* **1993**, *64*, 2892.

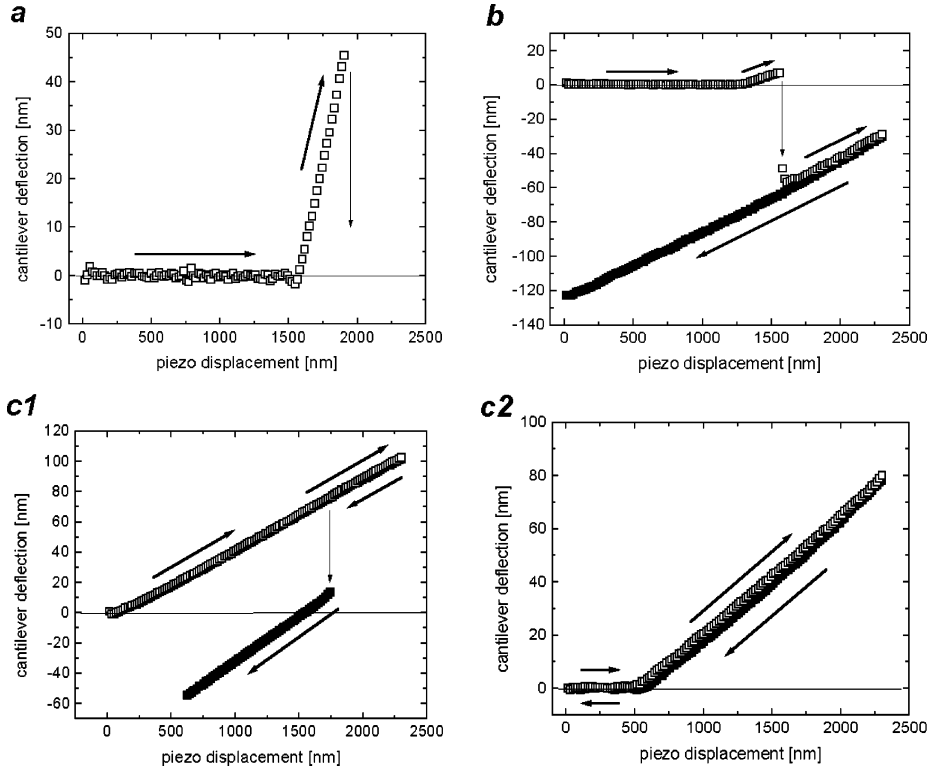

Figure 3. Typical $D-Z$ curves for water droplets in dodecane, as a function of surfactant concentration: 0.12 mM (a), 0.23 mM (b), and 2.33 mM (c1,c2). Approach curves, open symbols; retract curves, closed symbols. At the lowest Span 80 concentration, the retraction curve could not be registered as the probe was unable to snap out of contact. At the highest surfactant concentration, snap-in and snap-out events were only rarely observed. In panel c1, snap-in occurs upon retracting.

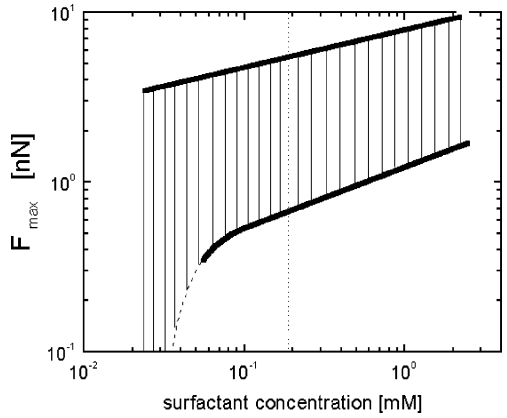

Figure 4. The maximum compression force measured just before the transition to probe−droplet contact (i.e., snap-in) varies with surfactant concentration. The range of F_{max} values is shown by the dashed area. The vertical dotted line indicates the cmc.

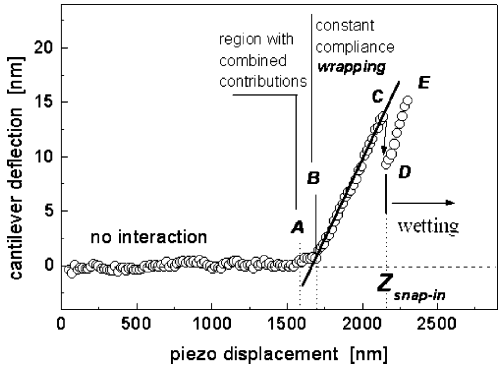

Figure 5. AFM $D-Z$ curve obtained on compressing (into) a water droplet (diameter, 120 μm) immersed in dodecane with 1.16 mM Span 80.

molecule (steric repulsion) and (b) the Laplace pressure becomes lower due to the reduced surface tension, leading to a more flexible surface. Both these effects are cooperative in preventing wetting (see eq 1).

The spread in F_{max} suggests that the transition from wrapping to wetting is a statistical event: apparently the jump from the former to the latter regime is governed not only by the force but also by a certain probability. We think that this probability depends on both the thickness of the oil film near wetting critical conditions and on the time during which these conditions apply. The occasional occurrence of snap-ins *on retraction* (as illustrated in Figure 3c1) corroborates the time aspect: it is hard to imagine that a gradual lowering of the compression force should induce wetting. A much more likely explanation is that an unstable interface has a certain lifetime due to unstable thermal fluctuations and needs some time to reach its stable (wetting) state.

The second aspect inspected was the slope of the $D-Z$ *curves* before wetting. To extract quantities with a physical meaning (like the droplet spring constant K_d) from these data, a few conceptual considerations are needed first. While some (weak) long-ranged repulsions appear to be present in our system (see for example Figure 5), we think that it is eventually the short-ranged *surfactant* contribution to Π which provides enough repulsion to enter the wrapping regime. Since our surfactant is nonionic, its effects on the disjoining pressure should be localized to 1−3 nm before contact between the probe and the droplet. In other words, the competition between the Laplace and disjoining pressures (wetting or wrapping) becomes only critical on a length scale comparable to the dimension of the Span 80 molecules. The implication of a negligible contribution of long-ranged (e.g., electrostatic) repulsions is that the total deformation can be attributed almost

completely to the droplet itself. Essentially it is the deformation of the droplet surface that is probed by our AFM experiments.

The implication for analyzing the $D-Z$ curves is that the slope just before the snap-in point provides the best measure for the droplet spring constant. At smaller compressions, also other contributions may have to be reckoned with (to be elaborated further on). In what follows, we shall discuss the *equivalent spring model* for droplets[4−6,11,14,15,18,21,22] and the corresponding procedure for data processing. Scrutinizing all data sets, for each single $D-Z$ curve it was possible to make a distinction between four main regions (see Figure 5). In the first region (up to point A), the colloidal probe is far from the droplet and no interaction is sensed (i.e., zero cantilever deflection). As the glass particle is brought closer to the droplet, the cantilever deflects from its equilibrium position due to the probe−droplet interaction(s). In this second region (region A−B), the cantilever deflection is determined by the interplay between three forces: one generated by the probe−droplet interaction (through the oil/surfactant medium), one due to droplet deformation, and one pertaining to the bending of the cantilever. They can be seen as three serial springs, each of them transmitting the same force. Generally, the colloidal interaction corresponds to a (highly) nonlinear spring.

At larger displacements, a third, *constant compliance region* (region B−C) is observed, i.e., the cantilever deflection increases linearly with the piezo displacement. In the literature, this behavior has been captured by considering the droplet as a linear spring, serially connected to the cantilever spring. For systems in which also colloidal forces are present, the corresponding "colloidal spring" can be left out from the modeling if, in the part of the $D-Z$ curve that is analyzed, any further compliance of this particular spring can be neglected. We believe that for our system this is the case. Under these assumptions, the droplet spring constant K_d can be calculated from

$$K_d = K_c \frac{S}{1-S} \tag{5}$$

where K_c is the cantilever spring constant and S is the slope of the $D-Z$ curve. One question was, which part of the $D-Z$ curve to select for measuring this slope. In line with the foregoing discussion, we have started our fitting at the point just before snap-in, working back from there to smaller deflections. Linear fits were made, starting from $Z_{snap-in}$ and going down in Z until the local derivative of the $D-Z$ curve diverged by a factor of 2 from average, followed by a linear regression on the first 30% of the points to determine the slope at maximum compression.

The linearity of the fitted part was also checked by fitting the experimental data with a power-law dependence: here we found exponent values between 1.0 and 1.1. The obtained slopes from the linear fits were plotted as histograms (not shown), averaged, and translated into K_d values using eq 5.

The dependence of these K_d values on the Span 80 concentration is shown in Figure 6a. On increasing the surfactant concentration, K_d initially shows a decrease and then saturates to a minimum value. Given the similarity of this behavior to that of the interfacial tension (γ) and in view of the presented theory, it is interesting to compare our K_d data with γ values taken from the literature.

According to Oliveira[32] and Li,[33] the interfacial tension at the water−dodecane interface is around 40−50 mN/m.

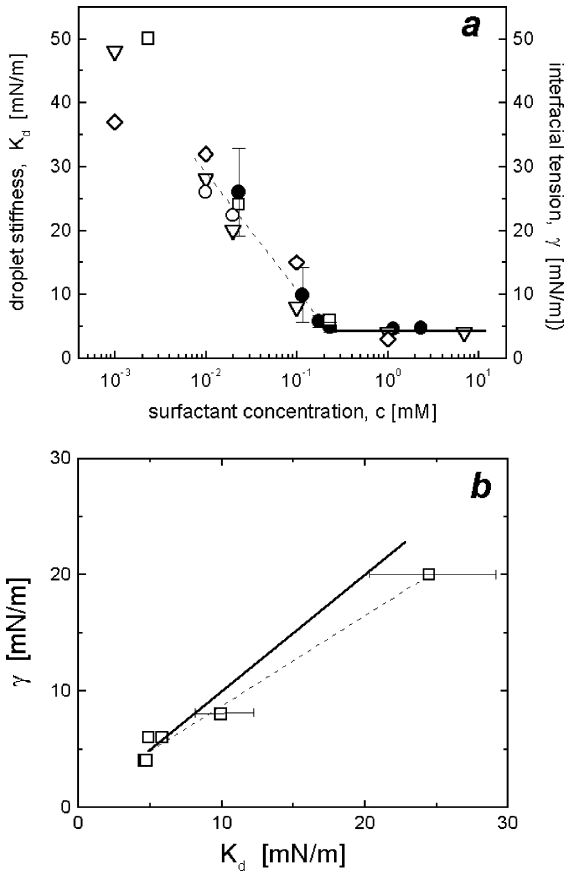

Figure 6. (a) Calculated values for the droplet stiffness (K_d, full symbols with error bars) versus the Span 80 concentration in bulk dodecane. Interfacial tensions (γ, open symbols) from the literature: down triangles, ref 28; diamonds, ref 29; squares, ref 30; and circles, ref 31. (b) Correspondence between our K_d values (symbols) and γ values interpolated from ref 28 to the same concentrations of Span 80. The drawn lines indicate $K_d = \gamma$ (full) and $K_d = 1.3\gamma$ (dashed).

For the same liquids, Peltonen et al.[31] measured $\gamma = 22.4$ mN/m in the presence of 0.019 mM Span 80 (their reported cmc). In the same paper, they showed that, for similar oils (like pentane, hexane, decane, etc.), the interfacial tensions and the corresponding cmc's have similar values. Remarkably enough, the cmc values found by Peltonen differ from those obtained by other investigators. For example, Evans[28] found for Span 80 in *n*-decane a cmc of 0.3 mM and a corresponding surface tension of $\gamma_{cmc} = 4$ mN/m. For Span 80 in hexadecane, Lobo[34] found $\gamma = 3.5$ mN/m for 23.3 mM surfactant. Campanelli[35] measured $\gamma = 5$ mN/m for 1.2 mM Span 80 in hexadecane (i.e., above their reported cmc of 0.8 mM). Valenzuela[29] found $\gamma \sim 4$ mN/m for 1 mM surfactant, and Opwale[30] found $\gamma = 6$ mN/m for 0.2 mM Span 80.

(28) Evans, G. M.; Habgood, M. G.; Boddy, G.; Galvin, K. P.; Biggs, S. R. *Proceedings of the Asian Pacific Confederation of Chemical Engineering Conference*, 2002 Christchurch, New Zealand.
(29) Valenzuela, F.; Salinas, C.; Basualto, C.; Sapag-Hagar, J.; Tapia, C. *J. Chil. Chem. Soc.* **2003**, *48* (1), 79.
(30) Opwale, F. O.; Burgess, D. J. *J. Colloid Interface Sci.* **1998**, *197*, 142.
(31) Peltonen, L.; Hirvonen, J.; Yliruusi, J. *J. Colloid Interface Sci.* **1998**, *240*, 272.
(32) Oliveira, R. C. G.; Gonzalez, G.; Oliveira, J. F. *Colloids Surf. A* **1999**, *154*, 127.
(33) Li, J.; Miller, R.; Wustneck, R.; Mohwald, H.; Neumann, A. W. *Colloids Surf. A* **1995**, *96*, 295.
(34) Lobo, L.; Svereika, A. *J. Colloid Interface Sci.* **2003**, *261*, 498.
(35) Campanelli, J. R.; Wang, X. *J. Colloid Interface Sci.* **1999**, *213*, 340.

For our oil/surfactant mixtures, we believe that the cmc must be close to 0.17 mM (0.0075 wt %), where the droplets' spring constant (roughly equivalent to the interfacial tension) reaches a saturation value. It is interesting to note that the threshold value associated with the appearance of spontaneous emulsification for pure water in dodecane/Span 80 falls in the same region, namely, C_w^{SE} = 0.14 mM (≈0.006 wt % Span 80).[26] This suggests that the SE mechanism must be connected with the drastic decrease of the interfacial tension (down to 4−5 mN/m) and the existence of surfactant micelles in the bulk dodecane.

One of our principal findings for the water droplets, shown by Figure 6a,b, is the good linear correlation between K_d and γ (from the literature). An unambiguous decision on the exact value of the prefactor cannot be made; both values (1.0 and 1.3) are suitable and correspond to a short-ranged (1−3 nm) repulsion in the context of the Attard model (see section 2). From this we conclude that for pure water droplets, the mechanical resistance against deformation is determined by the interfacial tension, if the steric barrier is sufficiently strong. Even if the steric barrier is weak (at low surfactant content) and jump-in events make it difficult to enter the *constant compliance regime*, the *equivalent spring* method can still be used to obtain a rough value for the interfacial tension.

4.1.3. Comparison of Different Probes. All data and calculations reported in the present work up to this point were related to experiments using one particular indenter (probe 1). To see whether our AFM measurements showed any dependence on the selected indenter, we also performed experiments (on selected formulations) using a different probe (probe 2). This latter probe had the same manufacturer specifications as probe 1 (although it came with a different batch) and was given the same cleaning treatment (see section 3.2).

Both panels a and b of Figure 7 show that apparent differences in surface properties for the two beads are not reflected in the *qualitative* dependence of the force-jumps on surfactant concentration. However, the magnitudes of the force-jumps for (a) the transition from wrapping to wetting and (b) the rupture of the droplet−probe contact in the retraction cycle clearly *do* show a dependence on the probe used. The fact that both the (average) $F_{snap\text{-}in}$ and $F_{snap\text{-}out}$ forces are significantly larger for probe 2 corroborates that both phenomena are related to wetting. Differences in local surface roughness or surfactant adsorption, or even different degrees of hydrophilicity of the glass particles used as probes, could all cause the difference between probe 1 and probe 2. However, it was beyond the purpose of this paper to study the cause of the difference in wetting in more depth.

Having established this remarkable difference between the two probes, we would like to stress here that other quantities (including the principal ones for the present study) were found *not* to depend on the used probe: (a) the general trends in the $D-Z$ curves (as discussed in section 4.1.1); (b) the K_d values extracted from the constant compliance regime, which varied only 10% or less between the two probes; and (c) the maximum force F_{max} at the end of the wrapping regime, which showed for both probes a variation as in Figure 4.

4.2. Deformation of Internally Gelled Droplets. In the experiments considered so far, the droplets' inner phase was always pure water. Below we report on the mechanical behavior of water droplets containing also gelatin in the inner phase (probe 1 was used as the indenter in all these experiments). By cooling a gelatin solution at a temperature below 30−35 °C, the molecules form cross-links and with time they build up a network (gel). The strength of the gel depends on both the gelatin concentration and the thermal history (i.e., setting temperature and aging). For a comprehensive review on these issues, the reader can consult the review of de Wolf.[37]

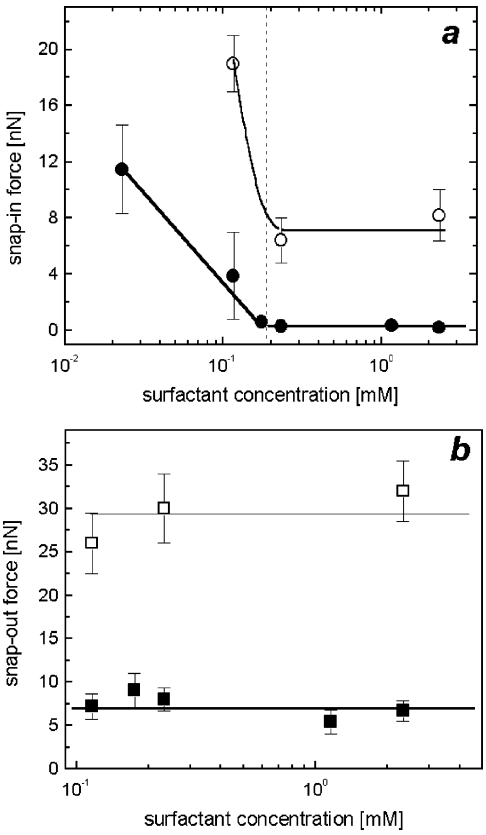

Figure 7. Force-jump magnitudes for the snap into contact (a) and snap out of contact (b) for pure water droplets: probe 1, full symbols; probe 2, open symbols. Forces higher than 22 nN were not determined from the software-registered AFM curves (due to a cutoff condition in the computer program). Instead, they were read as in voltages from an oscilloscope and converted into (nano)Newtons. Hence the error bars are larger (see the upper values in panel b).

4.2.1. General Features for $G_{10\%}$-Gelled Droplets. AFM $D-Z$ curves on droplets with 10% gelatin prepared in 0.023 mM Span 80/dodecane reveal a number of features which were also seen for the pure water droplets. Again, the approach curves ended with a snap-in (Figure 8a) and, on retraction, the capillary bridge between the droplet and the probe could not be ruptured by the software-controlled movement of the cantilever (release of the probe from contact had to be forced manually). Also for gelatin-containing droplets, a higher surfactant concentration in the oil helps to build a barrier against wetting. Most of the curves recorded above the cmc look like the ones in Figure 8b,c: snap-in (i.e., wetting) occurs at a large force (Figure 8b) or does not occur anymore (Figure 8c). By analyzing many $D-Z$ curves for each Span 80 concentration, the probability for snap-in could be also estimated here. The results shown in Figure 10c indicate that the frequency of the snap-in behavior falls on the trend observed for pure water.

Extending our analysis to the snap-in and snap-out force-jumps, more interesting information emerges. In the

(36) Preuss, M.; Butt, H.-J. *Int. J. Miner. Process.* **1999**, *56*, 99.
(37) de Wolf, F. A. Collagen and gelatin. In *Industrial Proteins in Perspective*; Aalbersberg, W. Y., et al., Eds.; Progress in Biotechnology, Vol. 23; Elsevier: Amsterdam, 2003; pp 133−218.

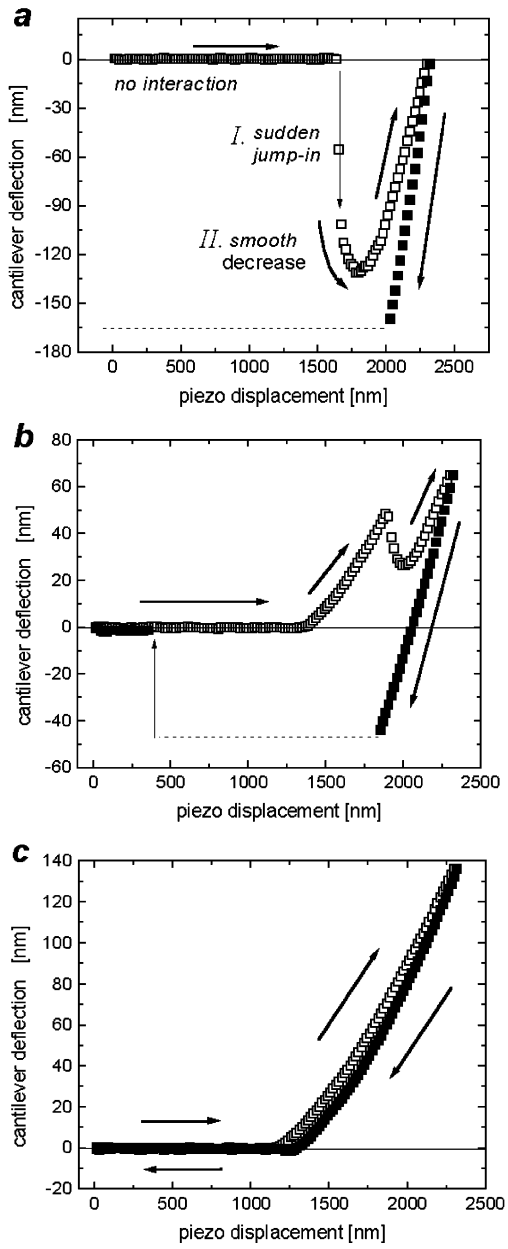

Figure 8. Typical $D-Z$ curves recorded during approach (open symbols) and retraction (closed symbols) on $G_{10\%}$-gelled droplets and two Span 80 concentrations: 0.023 mM (a) and 0.23 mM (b,c). Portions of the retraction curves (below the horizontal dotted lines) are not shown in the graphs.

presence of gelatin, the jump-in behavior consists in fact of two stages (best seen from Figure 8a): an instantaneous jump (true snap-in) (part I), followed by a more smooth approach of a local force minimum (part II). Since for pure water droplets part II was never observed, its origin must be related to the presence of gelatin inside the droplets. The duration of the process in part II was calculated to be 15−25 ms, after converting piezo displacements to real time using the approach speed. This number agrees in order of magnitude with the characteristic relaxation time of 4−8 ms observed in a previous AFM study on 10% gelatin samples.[38] We think that in both studies a viscoelastic response of the gelatin network was measured, but the volume of gelatin network and the strain involved may have been somewhat different.

(38) Uricanu, V. I.; Duits, M. H. G.; Nelissen, R. M. F.; Bennink, M. L.; Mellema, J. *Langmuir* **2003**, *19*, 8182.

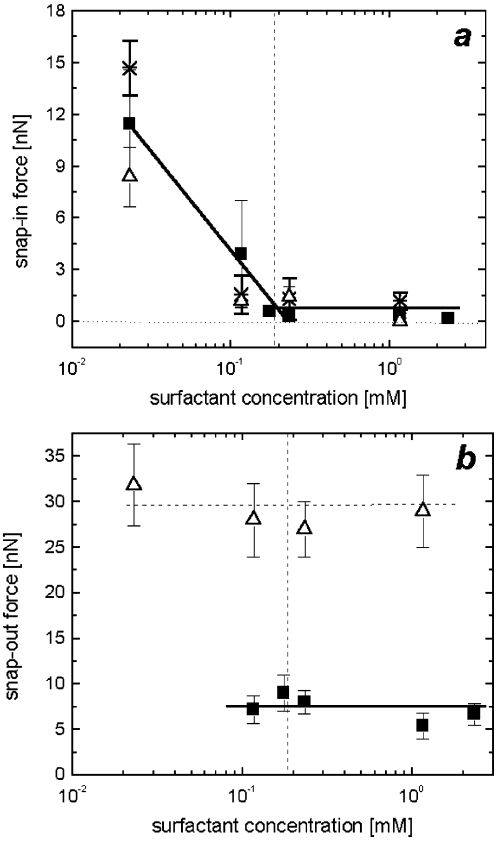

Figure 9. Snap-in (a) and snap-out (b) force-jumps measured on water (full symbols) or $G_{10\%}$ droplets (open symbols). The dotted vertical line indicates the cmc. In panel a, different symbols distinguish $F^{10\%\text{gel}}_{\text{snap-in/I}}$ (open) and $F^{10\%\text{gel}}_{\text{snap-in/total}}$ (stars).

Dividing the total force-jump from the snap-in critical point till the force minimum into the two parts as previously defined,

$$F_{\text{snap-in/total}} = F_{\text{snap-in/I}} + F_{\text{snap-in/II}}$$

the question arises, which of the force-jumps should be compared to the force-jumps for the pure water droplets. Depending on the mechanistic details of the wetting, either the part I or the total force could qualify for this: if one assumes that free (e.g., expelled) water at the gelatin/oil interface is responsible for snap-in, then the part I force should be most suitable. In the case that the probe gets wetted by a gelatin network, then the total force is most suitable. Based on Figure 9a, it is not possible to make a distinction. Regarding the *snap-out* behavior, Figure 9b illustrates that there are appreciable differences between the force-jumps measured for water and for gelled droplets, using the same probe.

4.2.2. Influence of Gelatin and Surfactant Concentrations on Wetting and Dewetting. Figures 9 and 10 present a mapping of the snap-in and snap-out behavior dependence on the gelatin and surfactant concentrations. Below we propose a qualitative picture which can explain the main trends. A very detailed explanation is not feasible in our opinion, considering the disbalance between the complexity (both the initial and the final state have to be considered, there may be a time dependence, and probabilistic elements can play a role) and the available information. Both the probability and the magnitude of the force-jumps should be considered. The snap-in and snap-out instabilities will be considered separately, as the mechanisms are partially different.

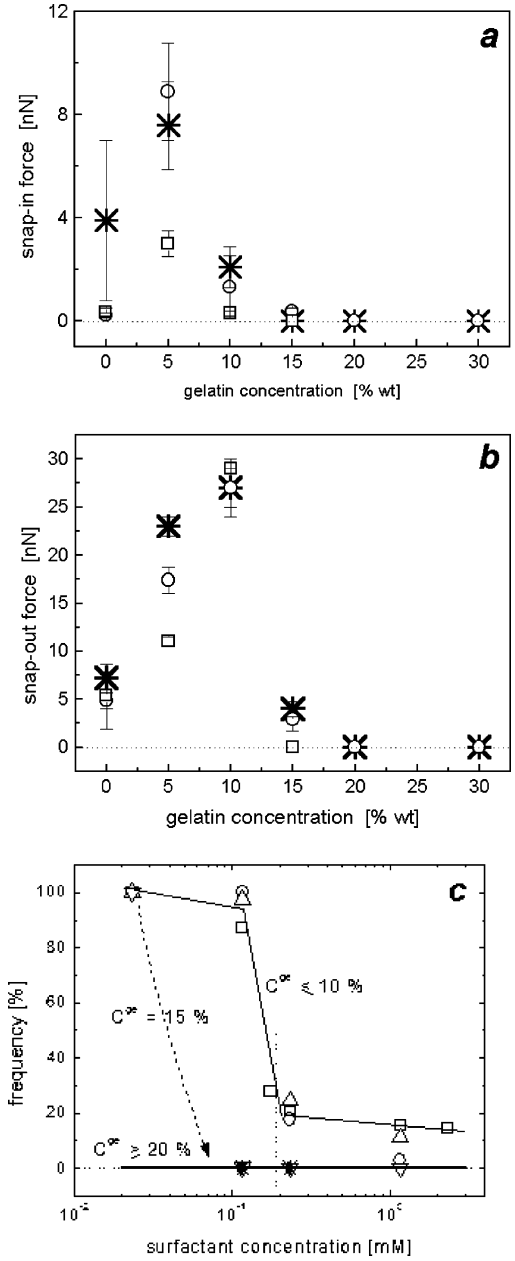

Figure 10. Snap-in (a) and snap-out (b) force-jumps measured on gelled droplets for 0.12 mM (stars), 0.23 mM (circles), and 1.16 mM (squares) Span 80. (c) Frequency of encountering a wetting instability, based on at least 250 $D-Z$ curves per composition. Lines are drawn to guide the eye. Legend: water (squares), 5% gelatin (up triangles), 10% gelatin (circles), 15% gelatin (down triangles), and 20% gelatin (stars).

For snap-in, two different possible mechanisms have to be distinguished: (1) colloidal attraction and (2) wetting. The first case applies for a minimum in the disjoining pressure curve (i.e., an attractive force, not preceded by a repulsion). This case should become apparent in the AFM curve as a snap-in starting at the $F = 0$ axis. Although a few such curves were encountered at very low Span 80 concentrations (see for example Figure 8a), most of our other experiments (for both water and gelled droplets) showed the $F \neq 0$ case. This fact suggests that wetting occurred, i.e., the repulsive disjoining pressure was not large enough to guarantee the stability of the oil film.

The probabilistic nature of the jump-in phenomenon is also consistent with wetting. Following eq 1, a probabilistic wetting should occur when the maximum disjoining pressure and the Laplace pressure are of comparable magnitude. In this regime, both changes in the maximum disjoining pressure and in the surface tension can affect the wetting probability. In this picture, increasing the Span 80 concentration should disfavor wetting along both ways, at least up to the cmc. The results of Figure 10c are in line with this.

The magnitude of the snap-in force-jump is set by the force difference between the repulsive state before wetting and the wetted state. Considering that the interfacial tension probably appears as a multiplicator both in the "critical wetting force" (see eq 1) and in the (quasi-equilibrium) "wetting force", one might expect a close-to-linear relation between the force-jump and the interfacial tension. This would explain the decreasing snap-in force up to the cmc in Figure 9a. Also the initial increase of the snap-in force with gelatin concentration in Figure 10a could be explained by this, considering that gelatin may partially displace Span 80 from the interface, thus raising the interfacial tension. In the presence of sufficient amounts of gelatin to obtain (visco)elastic droplets, the "wetting equilibrium" becomes modulated by the reduced compliance (or increased elastic resistance) of the droplets, having as a result a smaller contact area and a reduced wetting force. Increasing the gelatin content, the latter effect will eventually become dominant, and this explains the decrease in Figure 10a.

Snap-out occurs only if preceded by a snap-in (in the cases discussed here). For our system, it is related to a dewetting of the probe, via the breakage of the neck formed during probe retraction. Since the final state is a balance of forces, the critical snap-out force is equal to the jump amplitude. In principle, two failure mechanisms could play a role: an instability in the neck itself or an adhesive failure at the surface of the probe. In the first case, both the increased surface tension and the increased (visco)elasticity due to the gelatin could cause the initial increase of the snap-out force in Figure 10b. In the second case, an increased adhesion due to gelatin should be responsible. On the basis of our experiments, we cannot discriminate between the two situations. Also the difference in magnitude observed between water and 10% gelatin droplets in Figure 9b does not provide information about the nature of the jump-out mechanism. Irrespective of this, for both cases the explanation for the subsequent reduction of the snap-out force in Figure 10b is the same. The reduced contact area achieved in the compression stage, together with the reduced ability of the "neck" to recruit material from the "droplet", causes a decrease of the snap-out force. Eventually at still higher gelatin content the wetting becomes completely absent (as no snap-in occurs). This explains the maximum in Figure 10b.

4.2.3. Elastic Response of Gelled Droplets. In the foregoing sections, it was demonstrated that beyond certain (combinations of) Span 80 and gelatin concentrations, our droplets can resist deformation without wetting the probe. The corresponding $D-Z$ curves allow us to address one of the principal questions of this study: *which elastic response is obtained upon mechanical loading of a gelled droplet?* Aqueous droplets with gelatin in the bulk and enough Span 80 at the interface with the dodecane (so that the disjoining pressure is steep and droplets are in the wrapping regime) can resist deformation via both the interfacial tension and the bulk elasticity. The question is how these mechanisms work together. Let us first consider the two extreme cases. For pure water droplets, the *equivalent spring* model was seen to apply, with a good correspondence between the spring constant and the

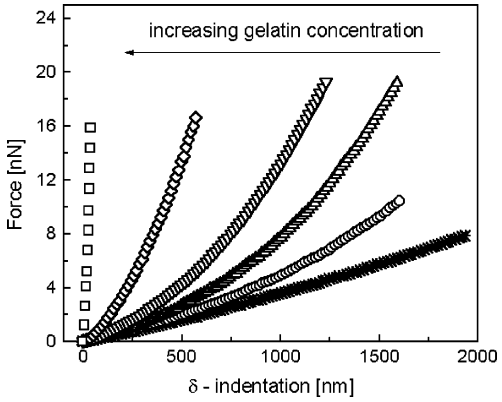

Figure 11. Force−indentation curves for droplets with various amounts of gelatin: 0% (stars), 5% (circles), 10% (up triangles), 15% (down triangles), 20% (diamonds), and 30% (squares). All samples were prepared with 0.23 mM Span 80. Note that for $G_{30\%}$ samples the $F-\delta$ curve cannot be distinguished from that of a hard substrate (using a cantilever with $K_c = 0.1$ N/m). Note also the increased resistance (maxima) compared to the water.

interfacial tension. For droplets with high gelatin concentration, one may expect an elastic response which is almost entirely due to the bulk modulus of the gel.

In the latter case, the Hertz model[39] could apply. In this model, linear elastic behavior is assumed, together with a smooth tip−sample contact during loading. The geometry of the indenter then determines the functional $F-\delta$ dependence, with δ being the indentation. For a spherical probe with radius R_p, the $F-\delta$ loading curve is described by

$$F = K_c D = \frac{4E^*}{3} R_p^{1/2} \delta^{3/2} \tag{6}$$

Fitting eq 6 to experimental $F-\delta$ curves, the relative elastic modulus (E^*) of the compressed material can be obtained. This approach requires the calculation of δ values from the $D-Z$ curves. For a purely elastic material (i.e., without any interactions prior to the direct contact between the indenter and the material), δ can be accurately defined as

$$\delta = (Z - Z_0) - D \tag{7}$$

with Z_0 the piezo displacement just before the first nonzero deflection in the approach curves and D the cantilever deflection. In our case, things are slightly more complicated due to the presence of colloidal interactions. Strictly speaking, one would need a model to take them into account and correct for their contribution to the overall deformation. In view of the large maximum forces applied in our compression experiments, we have ignored the colloidal contribution and defined δ as in eq 7.

A few representative $F-\delta$ curves for a given surfactant (0.23 mM) and different gelatin concentrations are shown in Figure 11. Adding more gelatin to the aqueous phase clearly increases the response level of the curves. Moreover, while the $F-\delta$ dependence for water looks linear, for gelled droplets the $F-\delta$ curve becomes noticeably curved.

To assess the extent to which the *linear spring* or the *Hertz* model could describe the data, we have attempted

(39) For a didactic presentation of the Hertz mechanical contact theory, the reader can consult: (a) Johnson, K. L. *Contact Mechanics*; Cambridge University Press: Cambridge, 1985. (b) Wang, Y. C.; Lakes, R. *Int. J. Solids Struct.* **2002**, *39*, 4825.

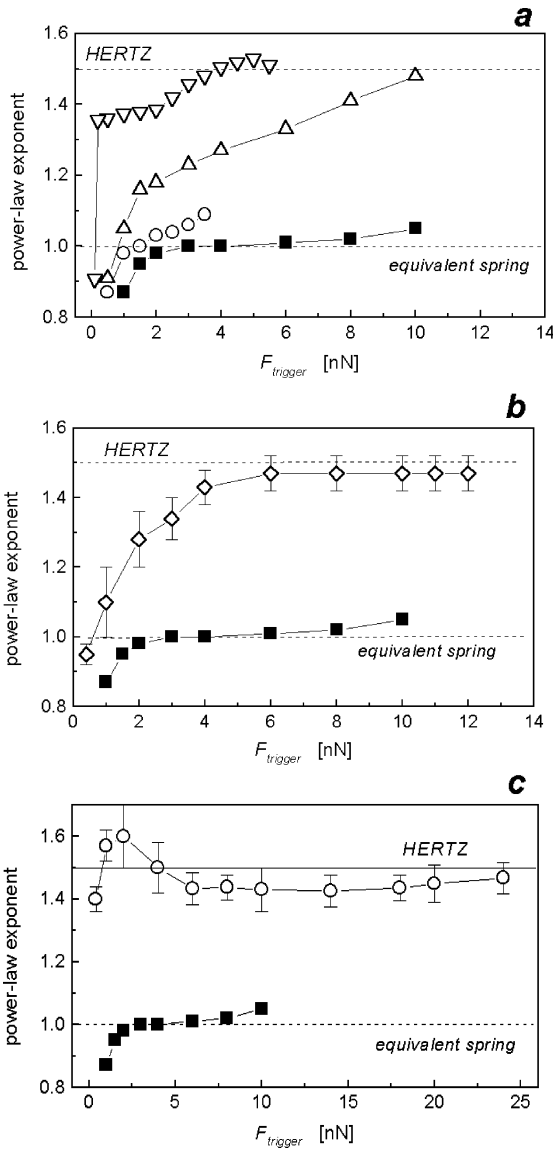

Figure 12. Calculated power-law exponents B based on fits using eq 8 and the variable-trigger approach (described in the text). Open symbols in each plot correspond to gelled droplets with 5% (a), 10% (b), and 15% (c) gelatin. Closed symbols represent pure water droplets, as a reference case. All samples were prepared with 0.23 mM Span 80. For $G_{5\%}$-gelled drops, a few individual B vs $F_{trigger}$ dependences are shown. For $G_{10\%}$ and $G_{15\%}$ droplets, averages over multiple B versus $F_{trigger}$ curves are presented.

to fit our $F-\delta$ curves with a general power-law function:

$$F = A\delta^B \tag{8}$$

where an exponent $B = 1$ corresponds to the linear spring model, while for $B = 1.5$ the Hertz model is recovered.

Analyzing all our experimental $F-\delta$ data with the fitting function (eq 8), the obtained exponent B was found to depend on the range of F values chosen for the fitting (especially for the 5% gelatin case). To analyze this dependence in more detail, we have followed a "variable-trigger" approach, in which each $F-\delta$ curve was subjected to a number of fits between $F = 0$ and $F_{trigger}$, taking the latter as a variable. The results are shown in Figure 12.

For pure water droplets, B reaches the value 1.0 at small indentations and remains constant thereafter: this corroborates the *equivalent linear spring* behavior (section

4.1). The B values below 1.0 might represent the influence of the colloidal force (region A−B in Figure 5).

A trend observed for gelatin contents below 15% (see Figure 12 a,b) is that there is not a single power law that fits the curves (the fit depends on the trigger point). For the $G_{5\%}$- and $G_{10\%}$-gelled droplets, B increases with $F_{trigger}$, starting around 0.9 and approaching a "saturation value" of 1.5. For the $G_{15\%}$ droplets, the latter value is reached already at small compressions. We explain this variation as being the result of the interplay between the interfacial tension and the bulk elasticity contributions. Under 15% gelatin, at small deformations the interfacial tension contributes to the droplet deformation and that determines the variation of the B exponent between the extreme values: 1.0 and 1.5 (Figure 12a,b). As deformation increases, bulk elasticity gains more and more influence, and from a certain point will start to dominate over the influence of the interfacial tension. At that point, B reaches the value 1.5 and stays constant for any deeper indentation. For 15% gelatin and above, the bulk elasticity is already so high that it dominates already for small indentations over the interfacial tension, the droplets behaving like pure elastic bodies for any indentation.

The $G_{5\%}$ droplets turned out to be a special case: in contrast to droplets at higher gelatin concentrations, there appeared to be appreciable scatter between different $B-F_{trigger}$ curves (three examples are presented in Figure 12a). Even so, the general trend is conserved: for a larger $F_{trigger}$, a higher power-law exponent is found. Also the mathematical dependence of individual curves suggests a complex behavior. For a low gelatin content like 5%, the probability of an inhomogeneous interface is higher. Gelled regions as well as "water pockets" might be present inside the droplet, near the interface. Having a weak network, water could also be easily expelled during the compression. Thus, pressing on such a surface can give various responses, depending whether there is only water contribution or also a contribution from the network inside. This could explain both the variation in the curve shape (as described by variation of the exponent B in Figure 12a) and the relatively good wettability of the probe (similar to the water case). On the other hand, for high gelatin concentrations, a denser, more homogeneous network reduces the number and size of possible water pockets and binds the water more strongly to the stiffer network (also via the hydrogen-bonding of the water molecules to the gelatin).

For droplets with gelatin concentrations above 5%, fitting the $F-\delta$ curves with a superposition of a linear and a Hertzian force law (corresponding to a parallel arrangement of springs) revealed that the Hertzian contribution was dominant. The relative Young moduli E^* obtained using the Hertz model for high indentations ($F_{trigger} = F_{max}$) for all $G_{10\%}$, $G_{15\%}$, and $G_{20\%}$ formulations are shown in Figure 13, along with a single result for a $G_{5\%}$ droplet (the upper curve in Figure 12a).

In this figure, also a comparison is made between the aforementioned E^*_{AFM} values and $E^*_{macrorheology}$, with the latter calculated from the G', the elastic storage moduli obtained from classical (i.e., macro) rheological measurements on bulk gels.[38] While the order of magnitude for the E^*_{AFM} and $E^*_{macrorheology}$ values is the same, there are obviously quantitative differences. Explaining these is beyond the scope of this paper (considering also that it has not been settled in the current literature that a quantitative correspondence should hold). However, the dependence of E^*_{AFM} on the amount of gelatin appears to be linear, and not with a power-law index of 1.8 as determined for macroscopic gelatin gels.[40]

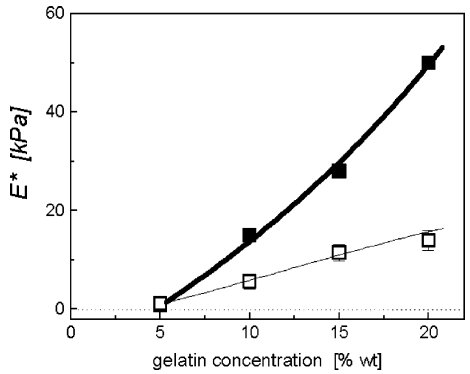

Figure 13. Relative Young moduli (E^*) determined using macrorheology (full symbols, ref 38) and AFM (open symbols) for several gelatin concentrations. The E^*_{AFM} values are calculated from compression curves for gelled droplets prepared with 0.23 mM Span 80.

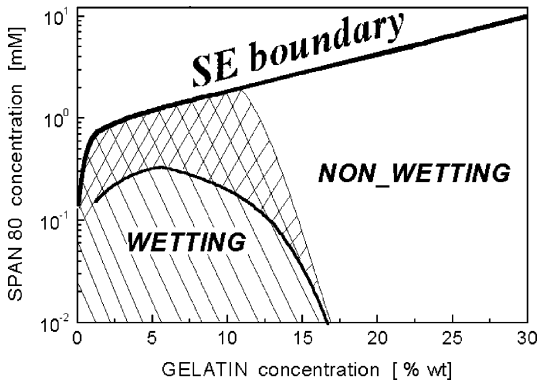

Figure 14. Stability diagram of emulsion droplets, mapped as a function of gelatin and surfactant concentrations. At high [Span 80], the droplets are affected by spontaneous emulsification. For low [gelatin] and/or [Span 80], the droplets show 100% wetting events (right-striped zone) or partial (i.e., smaller frequency) wetting (rombs zone). The diagram is semiquantitative, in that stability lines were generated from a limited number of observation points and could not always be sharply drawn.

4.3. Stability Diagram. The findings of the present AFM study (together with some additional observations) allowed us to make a semiquantitative mapping of droplet (in)stability areas as a function of gelatin and Span 80 concentration. The result is shown in Figure 14. Two kinds of interface instabilities were found in our experiments with single large droplets. The first instability concerns the wetting of a hydrophilic surface, measured with AFM. In assigning the (complete, partial, or non-) wetting areas in Figure 14, we have based ourselves on the wetting probabilities shown in Figure 10c. In the presence of gelatin, the probability for wetting was found to decrease. Up to a certain gelatin concentration, also the presence of surfactant was found to contribute to the prevention of wetting. The second instability concerns "spontaneous emulsification", that is, the formation of satellite emulsion droplets at the O/W interface of a mother droplet. We observed this with optical microscopy, above a certain surfactant concentration. Since the satellite droplet volume has to be made available from the inner phase of the mother droplet, one can expect that SE is also modulated by the presence of gelatin.

(40) Bot, A.; van Amerongen, I. A.; Groot, R. D.; Hoekstra, N. L.; Agterof, W. G. M. *Polym. Gels Networks* **1996**, *4*, 189.

The question now arises, how to connect the results of this study to stability issues (e.g., preventing coalescence) for real emulsions made from the same constituents. First of all, one should then consider whether a glass bead−droplet interaction is sufficiently similar to a droplet−droplet interaction. The hydrophilic nature of both glass and aqueous surfaces (in contrast with dodecane) speaks in favor of this assumption. Also the observed wetting behavior of the water droplets would support this view: the increased resistance against probe-wetting near the cmc (0.17 mM) correlates well with the general observation that in real emulsions, stability against coalescence is also obtained near this point.

Another factor to consider is that in real emulsions, the droplet size is typically between 1 and 10 microns. In principle, the droplet size will have an influence on the Laplace pressure, which plays a role in the wrapping-or-wetting issue (see eq 1). Considering the occurrence of a reduced radius in the expression for the Laplace pressure and the use of a 5 micron sized probe, the Laplace pressure for a pair of 10 micron droplets might be of comparable magnitude to those in our experiments (provided that nothing else but the size is changing, for much smaller droplets, the higher Laplace pressure should allow wetting at higher disjoining pressures, thus making them less stable).

Also the magnitudes of the forces have to be considered. Colloidal forces between the droplets in real emulsions are usually much smaller (e.g., 10−200 pN for depletion forces) than the typical compression forces (1−20 nN) applied in our AFM experiments. We remark here that such high forces could however be encountered in highly concentrated emulsions under strong shear flows. Since in our AFM experiments we found also a correlation between the wetting probability and the force applied, Figure 14 should in principle be given a third dimension, representing the force. Investigating this dimension would deserve further study.

5. Conclusions

We have studied the deformability of inverse (water-in-oil) emulsion droplets as a function of surfactant concentration using colloid-probe AFM in force−distance mode. The *equivalent spring* method was applied, after which the droplet spring constants were compared to literature values for the W/O interfacial tension. A good linear correlation was found, with a prefactor of 1.0−1.3, which suggests, in the context of the Attard model, that the *probe−droplet* repulsion which prevents wetting is short-ranged (1−3 nm). Thus it is possible to measure the surface tension of W/O droplets (semi-) quantitatively with AFM.

The mechanical resistance of water droplets against deformation is determined by the interfacial tension, but only if the surfactant layer at the droplet interface provides sufficient colloidal stability. At surfactant concentrations below the cmc this steric barrier is weak, and wetting of the probe occurs, manifested via jump-in events. While a frequent occurrence of the latter made it difficult to measure droplet spring constants at low surfactant concentrations, the method could still be used to obtain a rough value for the interfacial tension. The cmc of Span 80 in dodecane was found to be ≈0.17 mM.

We also studied the influence of bulk elasticity on the droplet deformation. Increasing the gelatin concentration makes the system more stable against wetting, as evidenced by a less frequent occurrence of snap-in events. Also the dependence on surfactant concentration diminishes for higher gelatin concentrations. The elastic response is strongly enhanced on adding gelatin, and also the shape of the force−distance curve becomes nonlinear. To assess the extent to which the *equivalent spring* or the *Hertz* model could describe the data, we have fitted our $F-\delta$ curves with a general power-law function.

Below 15% gelatin, for small enough indentations, the interface and bulk contributions to the elasticity are of a comparable magnitude. However, for deeper indentations the bulk elasticity becomes dominant, causing a Hertzian response. For droplets with higher (>15%) gelatin concentrations, a dominant Hertzian contribution was found for all indentations and did not depend on the surfactant concentration. The E^*_{AFM} values obtained using the Hertz model were of the same order of magnitude as the values obtained from macroscopic rheology experiments, but with a different concentration dependence.

Wetting of the probe turned out to be a complicating factor in the present study, especially at low surfactant and gelatin contents. Its probabilistic nature necessitated us to perform many experiments under these conditions. Its dependences on the particular probe used, droplet selected, or scan are still not fully elucidated but do not affect the main conclusions of the present paper. The influence of gelatin on (probe) wetting and dewetting was clearly manifested as a (visco-) elastic contribution to the snap-in and snap-out forces. The fact that even at high gelatin concentration wetting occasionally occurred suggests the presence of exudated (i.e., expelled by the gelatin network) water at the interface.

Acknowledgment. This work is part of the Softlink research program of the "Stichting voor Fundamenteel Onderzoek der Materie" (FOM). The research was possible due to financial support from Unilever, The Netherlands. Rob Vreeker (Unilever) and Dirk van den Ende (University of Twente) are kindly acknowledged for discussions and advice. The authors also thank Kees van der Werf and Martin Bennink for valuable technical support on the AFM instrument.

LA048276Y